Contents lists available at ScienceDirect

Surfaces and Interfaces

Tuning the adsorption of H_2O, H_2 and O_2 molecules on diamond surfaces by B-doping

Stefanos Giaremis , Maria Clelia Righi [*]

Department of Physics and Astronomy, University of Bologna, 40127 Bologna, Italy

ABSTRACT

In this study, the fundamental interactions between the low Miller index (001), (110) and (111) B-doped diamond surfaces and H_2O, H_2 and O_2 molecules, which are commonly present during growth, in ambient air and involved in electrochemical reactions, are investigated by means of *ab initio* simulations. The results are presented in close comparison with previous studies on undoped diamond surfaces to reveal the impact of B doping. It is demonstrated that the B dopant is preferably incorporated on the topmost carbon layer and enhances the adsorption of H_2O by forming a dative bond with O. On the contrary in some cases, it seems to weaken the adsorption of O_2, compared to the undoped diamond. Moreover, a noticeable displacement of the surface atoms attached to the fragment of the dissociated H_2O and O_2 molecules was observed, which can be associated to early stages of wear at the atomistic level. B doping was also found to reduce the energy barriers for water dissociation in most cases, with this effect being most pronounced in the C(111) surfaces. These qualitative and quantitative results aim to provide useful insights for the development of improved protective coatings and electrochemical devices.

1. Introduction

Diamond is extensively used in a wide variety of applications in materials science for its remarkable properties. Specifically, due to its ultrahigh hardness and excellent overall mechanical properties, micro- and nanocrystalline diamond is commonly used in the form protective thin film coatings grown usually with techniques such as chemical vapor deposition (CVD), for increasing wear resistance, for instance against erosion [1], scratch [2] and corrosion [3]. Surface functionalization by nanostructuring can also lead to interesting antibacterial and anti-biofouling properties [4]. Diamond like carbon (DLC) coatings are widely used in tribological applications. Carbon-based coatings in general yield low values of coefficient of friction (COF) and wear rates [5]. However, ambient conditions can deeply affect these tribological properties. In general, it is observed that the passivation of the carbon dangling bonds reduces the adhesive friction. Hydrogen termination was shown to reduce friction on diamond and DLC coatings, as well as dissociated H_2O [6–11]. For what concerns O_2 different results are reported in the literature: O_2 was found to increase friction and wear in some cases [12–14], but ultrathin nanodiamond films treated with oxygen plasma have been reported to present self-lubricating properties

(useful also for their self-cleaning and optical properties) [15].

The use of boron doped diamond is widely explored for several applications, ranging from tribology to biomedicine [16–18]. Different results are present in the literature on the effects of B dopants on friction and wear. It has been demonstrated that B-doped nanocrystalline films exhibit lower coefficients of friction than undoped ones, with the presence of B also associated to increased sp^3-to-sp^2 ratio [19]. Moreover, lower friction and wear rates were observed under water lubrication, compared to dry ambient conditions in Boron-Doped Diamond (BDD) films [20]. Appropriate surface texturing has been demonstrated to further improve the friction and wear behavior of BDD [17,20]. It is also observed that the tribological properties of BDD are sensitive to the B doping level. In DLC films with boron concentrations of 2.9 at.%, the friction coefficient was reduced compared to undoped DLC, though at a slightly elevated wear rate [18]. A threefold increase in wear rate with increasing B content from 0.6 at.% to 2.8 at.%, along with a decrease of hardness and elastic modulus in micro and nanocrystalline diamond on Si substrates was reported experimentally [21]. The authors report the presence of amorphization on wear tracks after ball-on-surface sliding tests, which they propose originates from weak lattice points due to the relatively weak B—B and B—C bonds. On the other hand, Lu et al.

fabricated microcrystalline BDD on cobalt-cemented tungsten carbide (WC—Co) with hot filament CVD (HCVD), exploring a B content range up to 1.5 at.%, demonstrating that a B content of 0.8 at.% was associated to the lowest COF and highest hardness and wear resistance [22]. Moreover, they found that this doping level led to the orientation of grains to the (110) direction, and that B atoms introduced a suitable amount of tensile stress to compensate the compressive stress of the diamond coating.

Another major field of application for BDD is in electrocatalytic applications, due to its electronic properties. Undoped diamond, despite presenting some very attractive properties such as low dielectric constant, extreme thermal conductivity (2200 $Wm^{-1}K^{-1}$ at room temperature), electron and hole mobility (4500 $cm^2V^{-1}s^{-1}$ and 3800 $cm^2V^{-1}s^{-1}$, respectively, at room temperature) and dielectric breakdown field (5–10 $MVcm^{-1}$), has also a wide bandgap (5.47 eV) and low electrical conductivity, which hinders its potential use in electronic devices [23]. Doping with B leads to a p-type behavior, adding acceptor states at about 0.4 eV above the valence band [24], and this is the most used strategy for tuning its electronic properties, as B presents a very low carrier activation energy (0.37 eV [25]). Doping with B content below $10^{19}cm^{-3}$ leads to clear valence band. A semiconductor-to-metal transition was theoretically predicted to occur at a B content of 2×10^{20} cm^{-3} [26] and experimentally, fast electron transfer indicating metallic behavior was observed at $1 - 4.5 \times 10^{20}$ cm^{-3} [27–29]. Moreover, since BDD presents other properties such as wide electrocatalytic window values (for instance, 4.9 V in ionic liquid, 4.6 V in organic solutions, 3.2 V in aqueous solutions) low, stable capacitance currents (3.6–7 µF cm-2 in aqueous, 14–20 µFcm^{-2} in organic and 11–15 µFcm^{-2} in ionic liquid solutions), high biocompatibility and chemical inertness in harsh environments (acidic or alkaline solutions, high voltages and current densities), it is very widely used in numerous applications in electrochemistry for electroanalysis, electrocatalysis/photoelectrocatalysis and electrosynthesis, biosensing and environmental purposes such as wastewater treatment and degradation of pollutants [30–34].

Atomistic scale effects are important for understanding the behavior of BDD in this type of applications. For instance, the presence of sp^3-bonded carbon was shown to be beneficial for the wide potential window due to the weak adsorption of intermediates during the H_2 and O_2 evolution reactions, and for the anticorrosion and antifouling properties due to the weak adsorption of other fouling species [35]. Moreover, the oxygen reduction reaction was proposed to occur preferably on the sp^3-bonded carbon component of electrodes [36]. High sp^2 concentration, on the other hand, was linked to a narrower window and surface oxidation [37]. Surface termination with H was linked to hydrophobicity, interfacial electron transfer, small potential window, and narrow bandgap with empty surface states while termination with O was linked to hydrophilicity and thus, higher background currents (due to the presence of water), wider potential windows and wide and clean bandgaps [34,38,39]. Hydrogen termination is known to lead also to the effect of negative electron affinity, i.e., the energy of the conduction band being higher than the vacuum level [40]. Hydroxyl is also used as surface termination, as a strategy for further reactions with other functional groups [41].

From the above, it is evident that the macroscopic properties of diamond and DLC coatings arise from the complex interplay of several factors, such as ambient conditions, crystallinity and grain size, bonding properties and the interaction strength between interfaces or surfaces and molecules. Therefore, assessing the impact of such atomistic-level mechanisms is important to the determination of the macroscopic behavior of BDD in scientific fields and applications such as those mentioned above. For this reason, atomistic simulations have been extensively used to unveil qualitatively and quantitatively relevant underlying phenomena. For instance, *ab initio* calculations have been used to compare the adsorption of water and hydrogen on the (2×1) Pandey reconstructed and unreconstructed diamond (111) surfaces, quantifying

the adsorption energetics and demonstrating that the latter becomes energetically preferable to the former for surface coverage greater than about 40 % due to chemisorbed adsorbents [42]. Similarly, the coverage of the (001) surface from the dissociative adsorption of atmospheric molecules and the associated potential energy surfaces were studied in [43]. The adsorption of water, hydrogen, and oxygen on the hydrogen and oxygen-terminated unreconstructed and Pandey reconstructed (111) surface orientations was investigated in [44], while the adsorption of the aforementioned molecules on the Pandey (001), (110) and (111) surfaces was examined in [45]. Density functional theory (DFT) calculations were also used to propose a theoretical model for the oxidation etching of the diamond (001) surface via the adsorption of the O_2 [46]. Recently, *ab initio* molecular dynamics simulations were used for examining the tribochemical reactions of H_2O, H_2 and O_2 on the diamond (111) and silica interface [47], as well as the water lubrication of sliding diamond surfaces through hydroxylation due to tribological effects [48]. The impact of B doping to the adsorption energies of hydrogen, oxygen, hydroxyl, and fluorine as surface-terminating species was explored by Zhao *et al.* [49], while the adsorption of the aforementioned molecules on the clean, B-doped (001) surface was investigated in [50]. The adsorption of water and hydroxyl radicals on hydrogen-terminated (111) surfaces was considered in [51]. *Ab initio* molecular dynamics on the interaction of the O- and H- terminated (111) and (001) BDD with water molecules was also used to assess the main factors of reactivity in each case [52].

However, while the adsorption of H_2O, H_2 and O_2 is extensively investigated, as mentioned above, a comprehensive analysis of the adsorption of these molecules on the clean, B-doped (001), (110) and (111) surfaces is not yet reported in the literature. Therefore, the results of DFT calculations are presented for the molecular and dissociative adsorption cases mentioned above, along with the respective energy barriers, in close comparison to previous theoretical results for the corresponding undoped surfaces [45]. Despite the fact that BDD is commonly H- or O- terminated, assessing the adsorption energetics of the clean surface can be relevant in scenarios involving low coverage of terminating species, due to previous reactions or removal due to wear or polishing. Moreover, BDD is initially H-terminated but H is being removed during growth via H abstraction reactions occuring in the gas phase [53,54]. Controlling the rate of the latter can modify the surface coverage during growth. Therefore, understanding the adsorption properties of the active sites on the clean surface obtained in such a manner can be also useful for subsequently controlling and modifying surface termination strategies. Overall, DFT simulations, as shown above, can demonstrate the impact of specific parameters, such as orientation and defects, to the desired property. Thus, despite the multiple structural phenomena that are present in a typical BDD surface, such as off-stoichiometric defects, grain boundaries, interstitials, and others, due to the non-equilibrium character of growth, in this work, the impact of the isolated component of the crystal orientation is determined. Moreover, such information has been shown to be invaluable for extracting conclusions for further macroscopic properties, such as wettability [55], thus it can hopefully motivate new strategies in areas such as thin films coating development for tribological applications, or improve, for instance, the current understanding of reaction pathways in electrochemical applications.

2. Computational details

All the DFT calculations were performed by using the QUANTUM ESPRESSO package [56] with the Vanderbilt ultrasoft pseudopotentials [57] based on the Perdew – Burke – Ernzerhof derivation of the generalized gradient approximation for the expression of the exchange correlation functional [58] and a cut-off energy of 30 Ry for the expansion of the plane-wave basis set. The semi-empirical D2 dispersion correction by Grimme [59,60] was applied to account for the long-range interactions between the surface and the considered molecules in the

physisorption states. This level of theory has been previously used in similar adsorption studies for undoped (e.g. [45,42,46]) and B-doped diamond surfaces (e.g. [50,51]) as a suitable trade-off between accuracy and computational cost. Moreover, calculations with the PBE functional were demonstrated to yield the same trends in the adsorption energies of the H_2O, H_2 and O_2 molecules and a similar level of accuracy compared to the PBEsol and PBE0 funtionals, for the adsorption of the aforementioned molecules in the undoped C(001), C(011) and Pandey C(111) surfaces [45], and also better agreement with experimental results compared to local-density approximation and Perdew-Wang 91 functionals [50]. Due to the presence of unpaired electrons from surface dangling bonds and molecular fragments, spin polarization was accounted for in all cases. A Gaussian smearing with a width of 0.01 Ry was applied for the integration of the Brillouin zone, which was sampled by a $2 \times 2 \times 1$ Monkhorst-Pack generated k-point mesh [61]. The convergence thresholds for the total energy and the ionic forces were set to 10^{-4} Ry and 10^{-3} Ry/Bohr, respectively, while the convergence threshold for the electronic self-consistent loop was set to 10^{-5} Ry. The most stable configurations for each adsorption case were determined by sampling a set of both of high and low symmetry positions for the initial positions of the corresponding molecule or fragments, respectively, and then comparing the total energies of the respective relaxed configurations. Consequently, adsorption energies (per molecule), E_{ads}, for both molecular and dissociative adsorptions, were calculated via $E_{ads} = E_{tot} - E_{surf} - E_{mol}$, where E_{tot} is the total energy of the adsorbate system, E_{surf} is the total energy of the clean, relaxed surface and E_{mol} is the energy of an isolated H_2O, H_2 or O_2 molecule, calculated on a $20 \times 20 \times 20$ cell. Visualizations were produced with XCrySDen [62].

Four different diamond surface configurations were considered, namely the C(001), the C(110), the unreconstructed C(111) and the Pandey reconstructed C(111), represented in orthorhombic periodic cells with a minimum lateral dimension of 8.75 Å, a minimum thickness of 6 atomic layers and a minimum vacuum size of 15 Å along the direction normal to the surface, to ensure that interactions between periodic images along this direction are negligible. The (2×1) dimer reconstruction was used for the C(001) surface, while for the case of the (111) surface, both the unreconstructed and the Pandey reconstructed cases were considered, since the reconstructed case is most likely to occur when the surface is not passivated (or, for instance, passivated with a hydrogen coverage below approximately 40 % [42]), but it was also computationally demonstrated that B as a dopant on the surface can have a stabilizing effect on the unreconstructed (111) surface [63]. The choice of cell dimensions was similar to [45] for the C(001), C(110) and Pandey C(111) configurations and similar to [47] for the unreconstructed C(111) configuration, and the simulation parameters were demonstrated to yield an energy error smaller than 3 meV. To investigate the local effects of B doping on atomistic level, on each configuration, one C atom was substituted with a B one, leading to a B concentration of 0.5–1.0 at.%. This choice is based on previous evidence that B in general favors substitutional doping [64], while more specifically, it has also been demonstrated from electron energy loss spectroscopy measurements that in the above concentration levels, B is found in the form of single and isolated substitutional atoms [65]. The respective concentration range used here is commonly referred to as "normal" or "medium" doping concentration level [66], and as mentioned above, is often used in studies regarding both tribological and electrochemical behavior.

Ab initio nudged elastic band (NEB) calculations [67] were also performed by using the Quantum ESPRESSO package [56] to examine the water dissociation pathways and energy barriers. The most stable molecular and dissociative adsorption states for water on each considered B-doped surface were considered as the initial and final images for the NEB calculations. All calculations were performed with the climbing image scheme [68] for determining the minimum energy path (MEP) for each reaction, and 8 interpolated images were used between the initial and final states, leading to a total number of 10 images for each reaction.

Results were compared with calculations for the respective undoped surfaces from [45] and [47].

3. Results and discussion

3.1. Structural properties of B-doped diamond surfaces

To investigate the energetically preferable site of the B dopant, substitutional sites at the three topmost (with respect to the exposed surface) atomic layers of each surface orientation were considered. The resulting configurations, along with the energy difference of each case compared to the energetically preferable one for each orientation, are presented in Fig. 1. For the (001), (110) and Pandey reconstructed (111) surfaces, B atom is preferable positioned on the topmost atomic layer. For these cases, sites deeper within the crystal lattice can be considered as metastable and will likely lead to the consequent diffusion of the dopant.

In the (001) surface, the B dopant on its most stable site is positioned on the surface dimer. Since B has only 3 electrons (compared to the 4 electrons of C), it forms single C—B bonds compared to the double C=C ones in the rest of the dimer chains. This is also evident from the breakdown of the C=C double bond (1.38 Å) to single B—C (1.57 Å) at the topmost layer. By evaluating the corresponding Löwdin partial charges, the B atom was found to be positively charged by +0.27e on its preferable position, while its three neighboring C atoms are negatively charged by −0.09e. This effect is reasonable considering the lower electronegativity of B compared to C (2.04 versus 2.55 Pauling units, respectively [69]). These results agree with previous *ab initio* studies that also confirmed the tendency of B to occupy sp^2-bonded sites at the topmost surface layer [50,70].

In the (110) surface, it can be assumed from their respective bond length (1.44 Å), that dangling bonds at the surface C atoms are being saturated by the formation of π-like or hybrid C—C chains. As in the previous case, the B dopant is also most stable at the topmost atomic layer for the (110) surface, with the same distribution of Löwdin partial charges between the dopant and its surrounding C atoms as in the (100) surface (+0.27e for B and −0.09e for its surrounding C atoms). The B—C bond length in the most stable site is 1.51 Å, so in this case, the preference of B atom for the topmost site can be also explained in terms of stress accommodation, as the elongation of the bonds that it is associated to, in this case, matches more closely the bond length of the diamond structure.

For the case of the Pandey reconstructed (111) surface, B atom prefers the site on the dimer chain, following the same trend as in the (001) surface. The B—C bond length in the dimer chain is 1.53 Å, while the respective one for the C—C bond in the chain is 1.43 Å. The Löwdin partial charge attributed to B in this case is +0.15e. The two surrounding C atoms in the chain dimer present a partial charge of −0.09e. This slight imbalance in partial charges, besides the known limitations of this scheme, can be also attributed to a small amount of charge transfer from the trench C atoms in the second atomic layer towards the ones in the surface chain dimers, as for the undoped surface, the former yields a value of +0.04e and the later a value of +0.01e. The presence of B on the topmost dimer chain was also associated with the lowest value of surface energy in a previous *ab initio* study [63]. The bond lengths in the top C—C dimer chains for the (001), (110) and Pandey reconstructed (111) surface are in agreement with previous *ab initio* works at the same level of theory [45].

On the other hand, in the case of the unreconstructed (111) surface, the B atom is most stable at the third atomic layer, as also previously shown from *ab initio* simulations [51] in the H-terminated BDD C(111) surface. It has been also reported, though, that B is most stable in the second layer in the H-terminated C(111) system, from DFT calculations at a different level of theory [71]. For this surface orientation, in all the B-doped cases, as well as in the undoped one, the top bilayer appears slightly compressed, with a C—C bond length of 1.50 Å, while its bonds
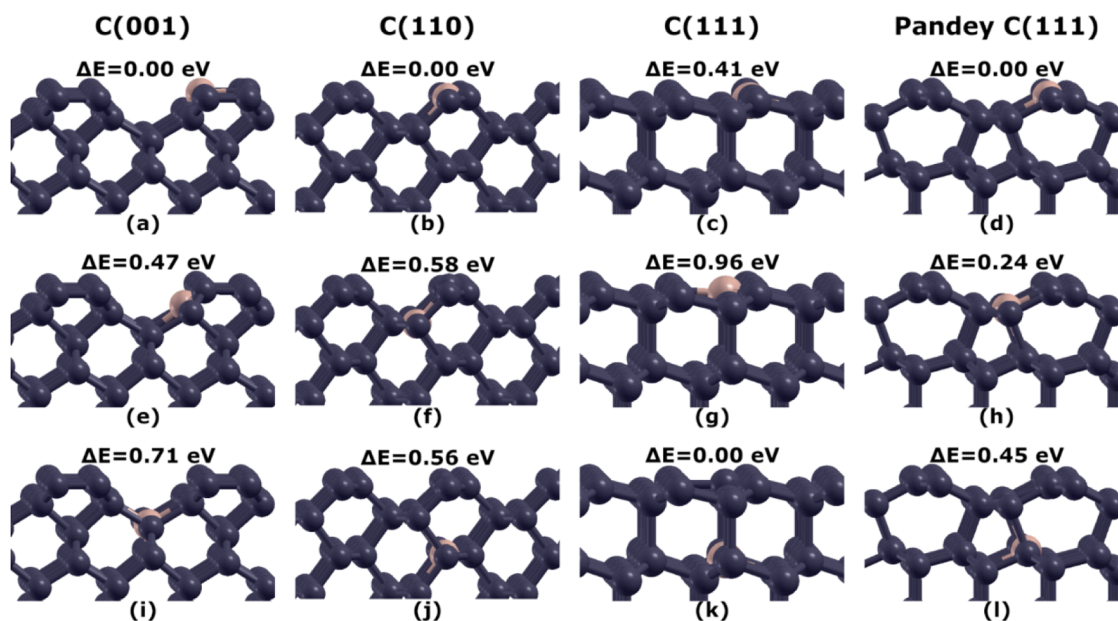
Fig. 1. Relaxed configurations of the B-doped surface models with the B atom on the first (a-d), second (e-h) and third (i-l) atomic layers from the surface, along with their respective energy difference, ΔE, compared to the energetically preferable configuration for each surface orientation, for the four considered surface orientations. Pink spheres correspond to the B dopants while grey spheres correspond to C atoms.

with the third atomic layer are slightly elongated at 1.65 Å. This slight tendency of the unreconstructed (111) surface towards graphitization is also reported in a previous *ab initio* study [51]. The tendency of the B atom to be substitutionally placed towards bulk lattice sites was also previously computationally demonstrated [70]. In its less stable sites at the first two atomic layers, B atom is found to form B—C bonds with a length of 1.53 and 1.52 Å, respectively, while in the most stable site at the third atomic layer, it actually forms bonds that match very closely the bond length of diamond (1.55 Å), while the respective C—C bond length in the same atomic layer in the undoped surface was 1.54 Å. In the latter case, the C atom on the second atomic layer that lies on top of the B dopant, is found to be shifted by 0.36 Å compared to the rest of the C atoms in the same layer, leading to a separation distance of 2.10 Å from the B atom underneath it. This effect can be explained by the fact that B has 3 electrons, therefore it forms three covalent bonds with the three neighboring C atoms in the fourth atomic layer, but it is weakly bonded with its fourth neighboring C atom on second atomic layer on top of it. The former, consequently, forms shorter, π-like bonds, with a length of 1.45 Å, with its three neighboring C atoms on the surface layer. This local bonding effect was also observed in [51]. The associated Löwdin partial charge of the B atom was found to be +0.16e at its most stable site at the third layer and +0.32e at the topmost site.

3.2. Molecular adsorption on B-doped diamond surfaces

The most stable configurations for the molecular adsorption of the H_2O, H_2 and O_2 molecules on the B-doped diamond (001), (110) unreconstructed and Pandey reconstructed (111) surfaces, with the B dopant on the topmost layer are presented in Fig. 2. However, as mentioned above, for the case of the unreconstructed (111) surface, the B dopant is preferably positioned in the third atomic layer. Moreover, as the case of the undoped unreconstructed C(111) surface was not considered in [45], the cases of the adsorption of the H_2O, H_2 and O_2 molecules on the unreconstructed C(111) surface with the B dopant on the third atomic layer (denoted as "B3") and the undoped unreconstructed C(111) surface, where explicitly investigated for completeness, and the respective results of molecular adsorption are presented in Fig. 3. The adsorption energies of the above cases are demonstrated in comparison with the ones of the respective undoped surfaces from [45] in Fig. 6a, while the

average adsorption energies for each molecule over all the considered surface orientations are presented in Table 4.

3.2.1. H_2O adsorption

The most evident impact of the presence of the B dopant on the topmost layer of all the considered diamond surfaces is towards the molecular adsorption of the H_2O molecule, as in this case, the surface-molecule interaction takes the form of chemisorption, while for the respective undoped surfaces, it has been computationally demonstrated to lead to a weak physisorption [45,42]. As previously computationally demonstrated but only for the (001) surface [50], the surface B atom tends to create a dative bond with the O atom of the H_2O molecule, which is associated to a pronounced energy gain due to the filling of the B outer shell. From Fig. 2 (a-d), it is evident that this also holds for the cases of the (110) and unreconstructed (111) orientations. The corresponding value of the adsorption energy per molecule, E_{ads}, for the (001) surface was found to be more slightly more pronounced, compared to the respective value for the (110) and the unreconstructed (111) configurations, while also the bond length between B and O follows the same trend (Table 1). From the Löwdin partial charge analysis (Table 1), it is evident that in all cases the B atom becomes less positively charged after the interaction with the H_2O molecule, while the O atom becomes less negatively charged.

Moreover, for the case of the unreconstructed (111) surface, when B is in the third atomic layer (which was found to be its most stable site), the molecular adsorption of H_2O becomes effectively similar to the respective case for the undoped surface. The adsorption energy per molecule for the former case (−0.20 eV) can even potentially indicate a slightly less favorable adsorption tendency compared to the latter one (−0.23 eV). The results for the undoped case are also in good agreement with a previous ab initio study [42]. The distance between the lowermost H atom of the H_2O molecule and the topmost atom of the BDD surface was 2.35 Å in the former and 2.37 Å in the latter case. The adsorption energy for the undoped case is also in good agreement with the results of Levita et al. (−0.22 eV) [42], while the weakening of the adsorption interaction between BDD and H_2O with increasing depth of the B dopant in this surface configuration was also previously reported from *ab initio* simulations with the PBE-D2 approach [51].

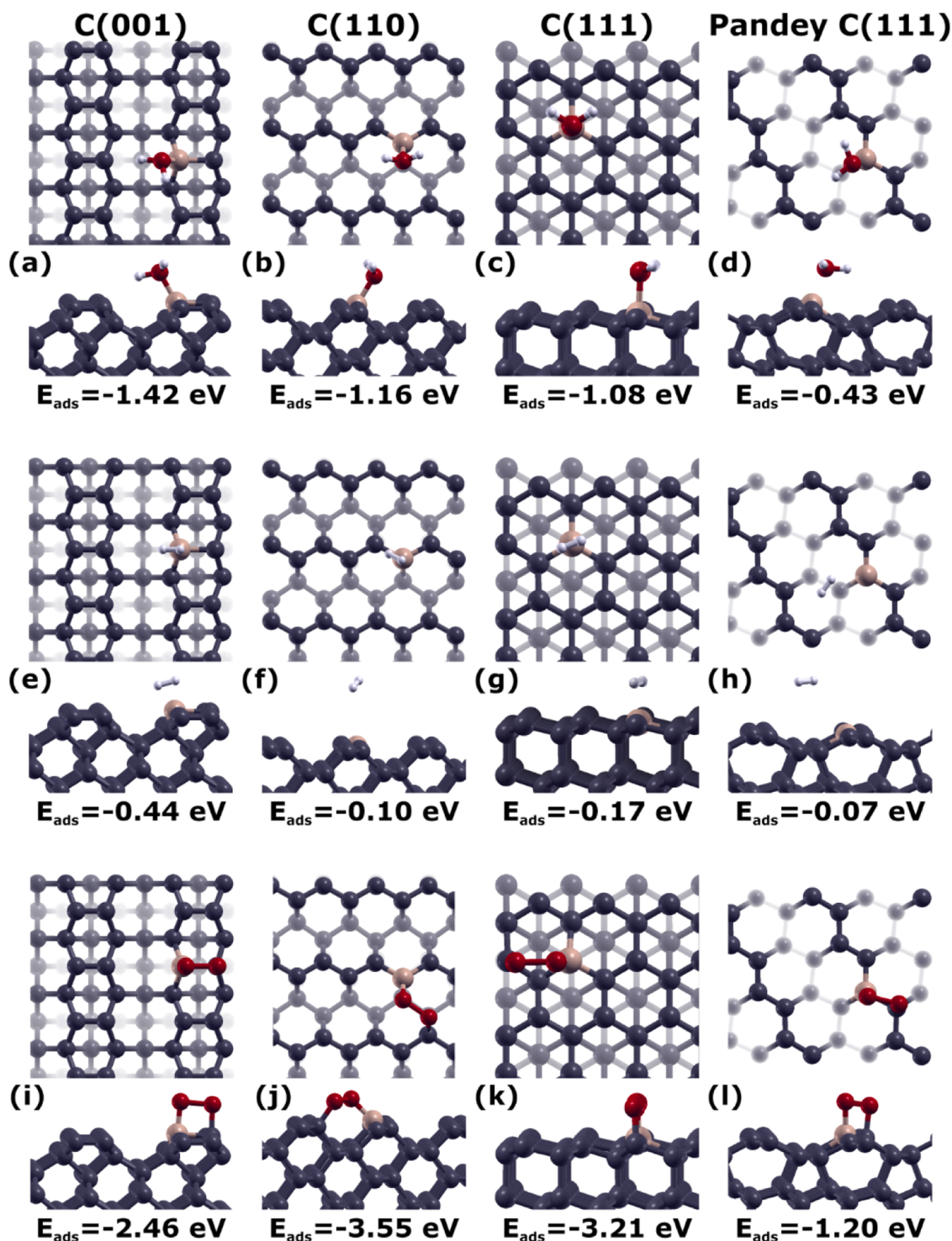The molecular adsorption of water on the Pandey reconstructed

Fig. 2. Top and side view representations of the most stable configurations for the molecular adsorption of the H_2O (a-d), H_2 (e-h) and O_2 (i-l) molecules, along with their respective adsorption energies per molecule, for the four considered surface orientations. Pink spheres correspond to the B dopants while grey spheres correspond to C atoms. H and O atoms are represented with white and red spheres, respectively. In all cases, the B dopant is positioned on the topmost atomic layer.

(111) surface is weaker compared to the previous cases, with the interaction being closer to a physisorption. This is evident by the lower energy gain, ($E_{ads} = -0.43$ eV for the B-doped versus -0.23 eV for the undoped surface), and the longer distance between the B and O atoms in the most stable configuration (1.77 Å). The Löwdin partial charge of the B atom is virtually the same before and after the interaction with the H_2O molecule (Table 1).

Overall, from the adsorption energies of the above cases, it is evident

that the molecular adsorption of H_2O is stronger on the (001) surface of BDD, while for the undoped diamond, it has been demonstrated that the adsorption was stronger on the (110) surface [45]. The order of reactivity for this type of adsorption on the B-doped surfaces was (001) > (110) > unreconstructed (111) (B1) > Pandey (111) > unreconstructed (111) (B3). Furthermore, by considering the average adsorption energies on all surface orientations (Table 4), it is evident that the impact of B is mostly pronounced in this type of adsorption, leading to an
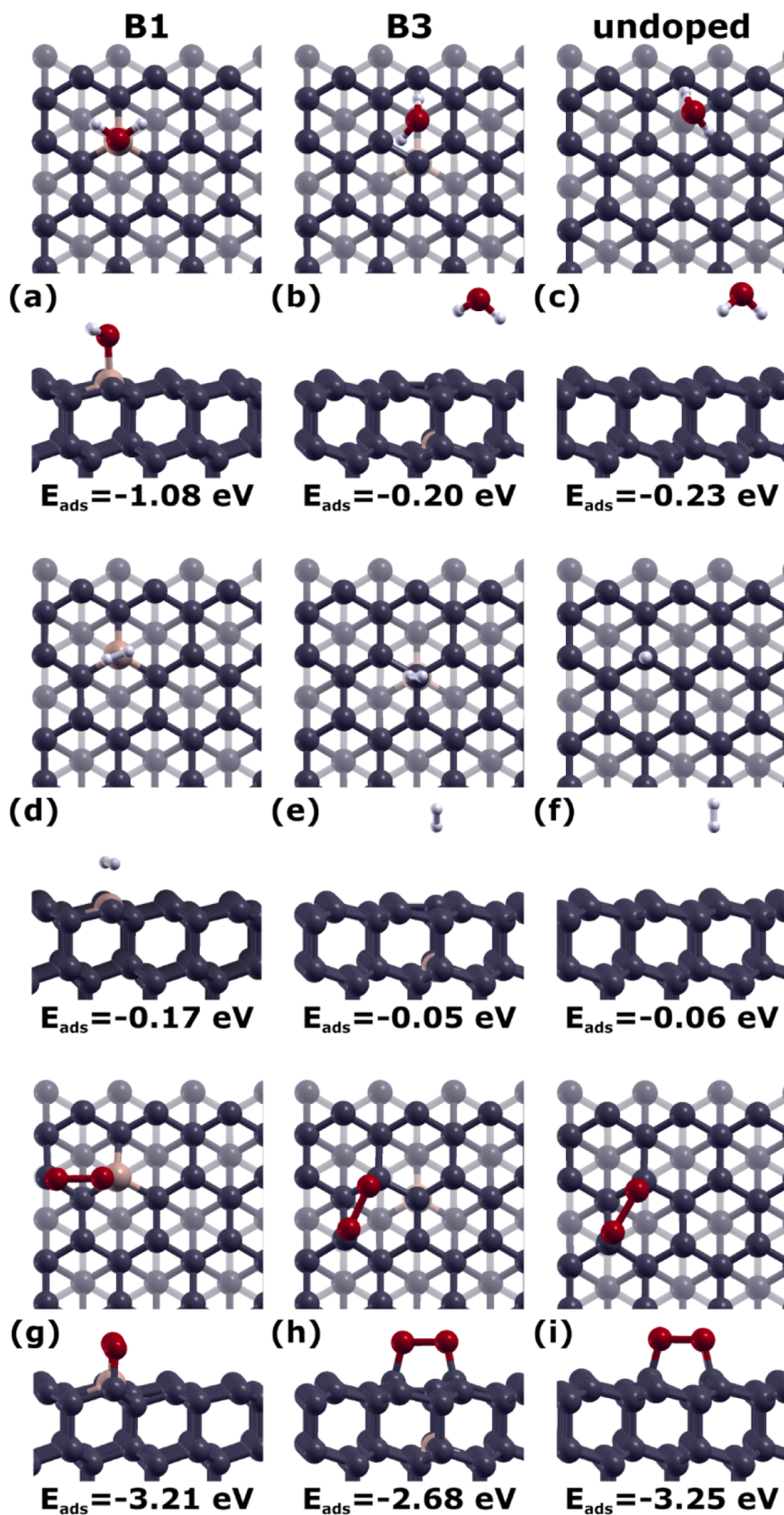
Fig. 3. Top and side view representations of the most stable configurations for the molecular adsorption of the H$_2$O (a-c), H$_2$ (d-f) and O$_2$ (g-i) molecules, along with their respective adsorption energies per molecule, for the B-doped, unreconstructed C(111) surface with the B atom on the first ("B1") and third ("B3") atomic layer, and the undoped unreconstructed C(111) surface. Pink spheres correspond to the B dopants while grey spheres correspond to C atoms. H and O atoms are represented with white and red spheres, respectively.

Table 1

Values of Löwdin partial charges of B and O before and after adsorption, and B—O bond length for the most stable configurations of molecular adsorption of H_2O on the B-doped (001), (110), unreconstructed and Pandey reconstructed (111) surfaces.

	(001)	(110)	(111)-B1	Pandey (111)
B partial charge (before adsorption) (e)	+0.27	+0.27	+0.32	+0.15
(after adsorption) (e)	+0.24	+0.16	+0.20	+0.16
O partial charge (before adsorption) (e)	−0.73	−0.73	−0.73	−0.73
(after adsorption) (e)	−0.56	−0.44	−0.45	−0.49
B—O (Å)	1.61	1.62	1.65	1.77

average increase of the respective energy gain by almost 0.7 eV with respect to the undoped case. The increased energy gain for the molecular adsorption of H_2O can be also associated to an increased probability of a H_2O molecule being captured from the surface. The attraction of H_2O molecules towards the B-doped diamond surface may be favor the surface oxidation with negative effects on its resistance to wear. On the contrary the increased surface hydrophilicity can be linked to the lower coefficients of friction observed under water lubrication [20], and to the attractive properties of BDD for use in electrochemical applications such as wastewater treatment [32].

3.2.2. H_2 adsorption

As for the case of the H_2O molecule, the molecular adsorption of H_2 from the undoped diamond surface has been previously computationally demonstrated to take the form of physical adsorption [45]. The incorporation of B atom on the topmost layer changes this picture for the cases of the (001) and the unreconstructed (111) surfaces (Fig. 3e-h). In these cases, the adsorption becomes stronger, with the associated adsorption energies per molecule appearing increased, compared to the ones for the corresponding adsorptions on the undoped surfaces (−0.44 eV versus −0.07 eV from [45] for the (001) surface and −0.17 eV versus −0.07 eV from [45] for the unreconstructed (111) surface). For the (001) surface, there is a pronounced attraction of the H_2 molecule from the B dopant, as the configuration in its most stable state was found to lead to a chemisorption state by the formation of a dative B—H bond and the stretching of the H—H bond (Table 2). The adsorption appears less pronounced for the case of the unreconstructed (111) surface with the B dopant on the surface layer, as the energy gain was found to be less increased and a longer B—H dative bond was formed (Table 2). The stretching of the H—H bond was also less significant in this case (Table 2). In both cases, from the partial charge analysis, it was found that B was became less positively charged while H became more positively charged after adsorption, indicating a potential charge transfer towards B (Table 2).

The H_2 molecule was found to be physisorbed on the other two surfaces. The adsorption energy for the BDD (110) surface was slightly weaker compared to the undoped case, while the molecule was found to adsorb at 2.78 Å from the surface (measuring from the lowest H atom to the topmost surface atom). Finally, in the Pandey reconstructed (111)

Table 2

Values of Löwdin partial charges of B and H before and after adsorption, and B—H and H—H bond lengths for the most stable configurations of molecular adsorption of H_2 on the B-doped (001) and unreconstructed (111) surfaces.

	(001)	(111)-B1
B partial charge (before adsorption) (e)	+0.27	+0.32
(after adsorption) (e)	−0.04	+0.10
H partial charge (before adsorption) (e)	+0.04	+0.04
(after adsorption) (e)	+0.26	+0.20
B—H (Å)	1.40	1.57
H—H (Å)	0.84	0.78

surface, the adsorption energy on the doped surface was the same as in the undoped one, leading also to a weak physisorption, with the H_2 molecule in both cases being on top of the middle of a trench formation at 2.42 Å from the topmost surface atom.

Overall, the molecular adsorption of H_2 is weaker compared to the one of H_2O, which was also found to be the case for the respective undoped diamond surfaces [45]. However, the adsorption of H_2 was stronger on the (001) surface, as was also the case with H_2O, while for the undoped diamond surface the adsorption of H_2 was stronger on the (110) surface [45]. By also considering the average adsorption energies in Table 4, this type of adsorption is the weakest among the considered cases, with the addition of B leading to a small increase of energy gain by only approximately 0.08 eV in average.

3.2.3. O_2 adsorption

In contrast with H_2O and H_2, the molecular adsorption of O_2 from undoped diamond surfaces has been demonstrated to have a mostly chemical character [45]. Here, the presence of B as dopant in the topmost atomic layer is also found to lead to the chemisorption of the O_2 molecule in all the considered cases, with the O=O double bond being rearranged into single bonded O—O, C—O and B—O configurations.

Specifically, in the (001) surface, the O_2 molecule is preferably positioned on top of the B—C heterodimer, in similar manner to the case of the undoped surface [45]. The molecular adsorption of oxygen was found to be weaker compared to the undoped surface [45] by 1.24 eV. The adsorption of O_2 on the B-doped (110) surface was also found to occur in a similar manner to the undoped case [45], with O_2 being preferably chemisorbed in the middle of the trench and each O atom attached to either B or a C atom at the opposite side of the trench. The adsorption on the B-doped (110) surface was found to be weaker compared to the respective undoped one [45] by 0.9 eV.

The impact of surface B-doping on the O_2 adsorption was less pronounced for the two cases considered for the (111) orientation, as the calculated adsorption energies were found to be very close to their respective counterparts for the undoped configurations. For the Pandey reconstructed surface, O_2 was found to be favorably positioned on top of B and its neighboring C atom on the surface chain. In the unreconstructed (111) configuration, when B was positioned on its preferable site in the third atomic layer, O_2 was preferably chemisorbed far from the vicinity of B. As for the assessment of the local impact of B, only sites up to the second coordination shell of the dopant were considered, the preferable position of O_2 for the molecular adsorption was found to be in a manner such as one O atom was on top of a C atom in the second coordination shell of B and the second O further away from B (fourth coordination shell). This configuration leads to a weaker adsorption of the molecule compared to the undoped case. However, by moving the O_2 molecule further away from the vicinity of B, the adsorption energy tends to reach the value of the undoped configuration.

The results of the partial charge analysis in Table 3 indicate charge transfer towards O_2, which however occurs through the C atom in which O_2 is attached to, as the change of the partial charge of B before and after adsorption is less pronounced. Moreover, the B—O length was found to be longer in all cases compared the respective C—O one (Table 3), as expected.

Overall, the molecular adsorption of O_2 was found to be stronger on all the considered B-doped surfaces, compared to the molecular adsorption of H_2O and H_2, as was also the case for the respective undoped configurations [12]. Furthermore, again as in the undoped case, the (110) configuration was found to be more favorable towards this type of adsorption. However, the second most favorable surface was the unreconstructed (111) (B1) for the B-doped case but the (001) for the undoped one. The adsorption on the Pandey reconstructed (111) surface was the least favorable both in the B-doped and the undoped configuration, as was also the case for the rest of the considered molecules, in agreement with previous studies demonstrating the inert character of this surface [42]. The molecular adsorption of O_2 was found to be the

Table 3

Values of Löwdin partial charges of B, O attached to B (O_B), C and O attached to C (O_C), before and after adsorption, and B—O, C—O and O—O bond lengths for the most stable configurations of molecular adsorption of O_2 on the B-doped (001) and unreconstructed (111) surfaces.

	(001)	(110)	(111)-B1	Pandey (111)
B partial charge (before adsorption) (e)	+0.27	+0.27	+0.32	+0.15
(after adsorption) (e)	+0.22	+0.20	+0.20	+0.19
O_B partial charge (before adsorption) (e)	+0.05	+0.05	+0.05	+0.05
(after adsorption) (e)	−0.18	−0.20	−0.21	−0.22
C partial charge (before adsorption) (e)	−0.08	+0.01	+0.04	−0.09
(after adsorption) (e)	+0.09	+0.23	+0.25	+0.10
O_C partial charge (before adsorption) (e)	+0.05	+0.05	+0.05	+0.05
(after adsorption) (e)	−0.12	−0.15	−0.26	−0.14
B—O (Å)	1.51	1.47	1.49	1.55
C—O (Å)	1.47	1.46	1.44	1.49
O—O (Å)	1.48	1.49	1.59	1.48

strongest among the considered types of molecular adsorption, with the addition of B leading to a reduction of the average energy gain by 0.55 eV per molecule (Table 4). However, the large values of standard deviation reflect the impact of the different surface orientations mentioned above.

3.3. Dissociative adsorption on B-doped diamond surfaces

The most stable configurations for the fragments of H_2O, H_2 and O_2 dissociated on the B-doped surfaces having B in the first layer are presented in Fig. 4, along with the corresponding adsorption energies. For the unreconstructed (111) surface both the cases with B on the first ("B1") and ("third") atomic layers are considered and compared with the undoped one in Fig. 5. The dissociative adsorption energies are compared to those obtained for the undoped surfaces [45] in Fig. 6b. Overall, the impact of boron doping was less pronounced for the dissociative adsorption than for molecular adsorption.

3.3.1. H₂O dissociative adsorption

As in the undoped cases, the hydrogen and hydroxyl fragments occurring as products from the dissociative adsorption were found to be preferably adsorbed from the topmost chains and dimers, with the hydroxyl group being preferably adsorbed on the B atom by forming a dative bond, and the H atom being adsorbed by its adjacent C atom. This was observed in all configurations except for the unreconstructed (111) surface. In the latter, when B atom was positioned on the topmost layer ("B1" configuration), both fragments were found to be preferably attached to C atoms in the first coordination shell of B, while when B atom was positioned in its most stable position in the third layer ("B3" configuration), the hydroxyl fragment was preferably attached further away from the site on top of the B dopant. The value of the adsorption energy for the B1 case was found to be close to the one for the undoped one, which was also the lowest compared to the rest of the considered

Table 4

Average adsorption energies per molecule, along with the respective values of standard deviation in parentheses (all in eV), for each molecule, estimated over all the four considered surfaces. Results are presented both for the molecular and the dissociative adsorption of the considered molecules.

	Molecular adsorption		Dissociative adsorption	
	B-doped	undoped	B-doped	undoped
H_2O	1.02 (0.36)	0.34 (0.19)	2.75 (0.91)	2.61 (1.14)
H_2	0.20 (0.15)	0.12 (0.08)	3.45 (0.96)	3.49 (1.13)
O_2	2.61 (0.90)	3.15 (1.20)	4.04 (1.10)	4.40 (0.92)

surfaces. The results for the undoped surface are also in agreement with previous *ab initio* calculations [42]. The adsorption energy for the most stable configuration for the B3 case was higher, indicating a weaker adsorption on the surface near B, and thus the detrimental impact of B towards the H_2O dissociative adsorption in this case. However, this effect was local, as placing the fragments further away from the site on top of the B dopant, the value of the adsorption energy was found to reach rapidly the corresponding value for the undoped case.

In all the configurations, the OH group was preferably oriented pointing the H away from the H fragment due to the electrostatic repulsion between them. The strength of the adsorption was found to be relatively similar for the (001), (110) and the unreconstructed (111) orientations, with the energy gain decreasing for unreconstructed (111) (B1) > (110) > (001) > unreconstructed (111) (B3) > Pandey reconstructed (111). The B—O bond lengths reflect the above trend, with values of 1.40 – 1.43 Å for the unreconstructed (111), (110) and (001) surfaces and 1.48 Å for the Pandey reconstructed (111) surface. The adsorption on the Pandey reconstructed surface was weaker by almost 2 eV, demonstrating again the inert character of this configuration. The addition of B appears to favor the dissociative adsorption of H_2O in the Pandey configuration, as the energy gain was increased from 0.63 eV for the undoped surface to 1.18 eV for the B-doped one. The incorporation of B did not lead to any significant changes to the adsorption energies in the rest of the surface configurations, compared to their undoped counterparts. However, from Fig. 4(a-d), it is observed that the adsorption of the hydroxyl group on the B atom in the (001), (110) and Pandey reconstructed (111) surfaces leads to a displacement of the latter. This effect was less pronounced in similar calculations on the undoped surfaces [45], and it can be potentially associated to evidence of increased wear in BDD (e.g., [19]).

Overall, the dissociative adsorption of H_2O was found to be the weakest, compared to the dissociative adsorption of H_2 and O_2, both for the B-doped and the undoped surface orientations. The weak interaction of BDD with OH is also reported experimentally and is assumed in reaction pathways models for water oxidation, where hydroxyl intermediates are assumed to react weakly with the surface of the BDD electrodes [72,73].

3.3.2. H₂ dissociative adsorption

In the dissociative adsorption of H_2, the H fragments adsorb on the surface on the topmost chains and atomic layers in all the considered surfaces, forming single bonds with a length of 1.10 Å. In all cases, the H fragments were not preferably attached to the B dopant, but to its adjacent or next-to-adjacent C atoms. Specifically, the H atoms were preferably attached to the neighboring C atoms of the B dopant in the (110) and Pandey reconstructed (111) surfaces. In the (001) surface, one H atom was preferably adsorbed by the C atom on the B—C dimer and the other was adsorbed by a C atom on the adjacent dimer, rearranging the C═C double bond into a single C—C one. Lastly, in the unreconstructed (111) surface, H atoms were attached to C atoms in the second coordination layer of the B dopant.

Overall, the addition of B to the topmost layer was not found to have a very significant impact to this type of adsorption, as it was associated with a small decrease of the adsorption energy gain for the (001), (110) surface and unreconstructed (111) surfaces and an increase of the energy gain for the Pandey reconstructed (111) surface. The order of the adsorption energy gain for the dissociative adsorption of H_2 was found to be unreconstructed (111) (B1) > (110) > (001) > unreconstructed (111) (B3) > Pandey reconstructed (111).

The adsorption was found to be stronger on the unreconstructed (111) surface, with an energy gain of 4.12 eV for the B1 configuration. The very high energy gain for the unreconstructed (111) towards the H_2 dissociative adsorption agrees with the well-known ability of passivating this surface with H [74]. This effect is here demonstrated to hold also for the B-doped unreconstructed (111) surface. However, as in the case of the dissociative adsorption of H_2O, the incorporation of B in the
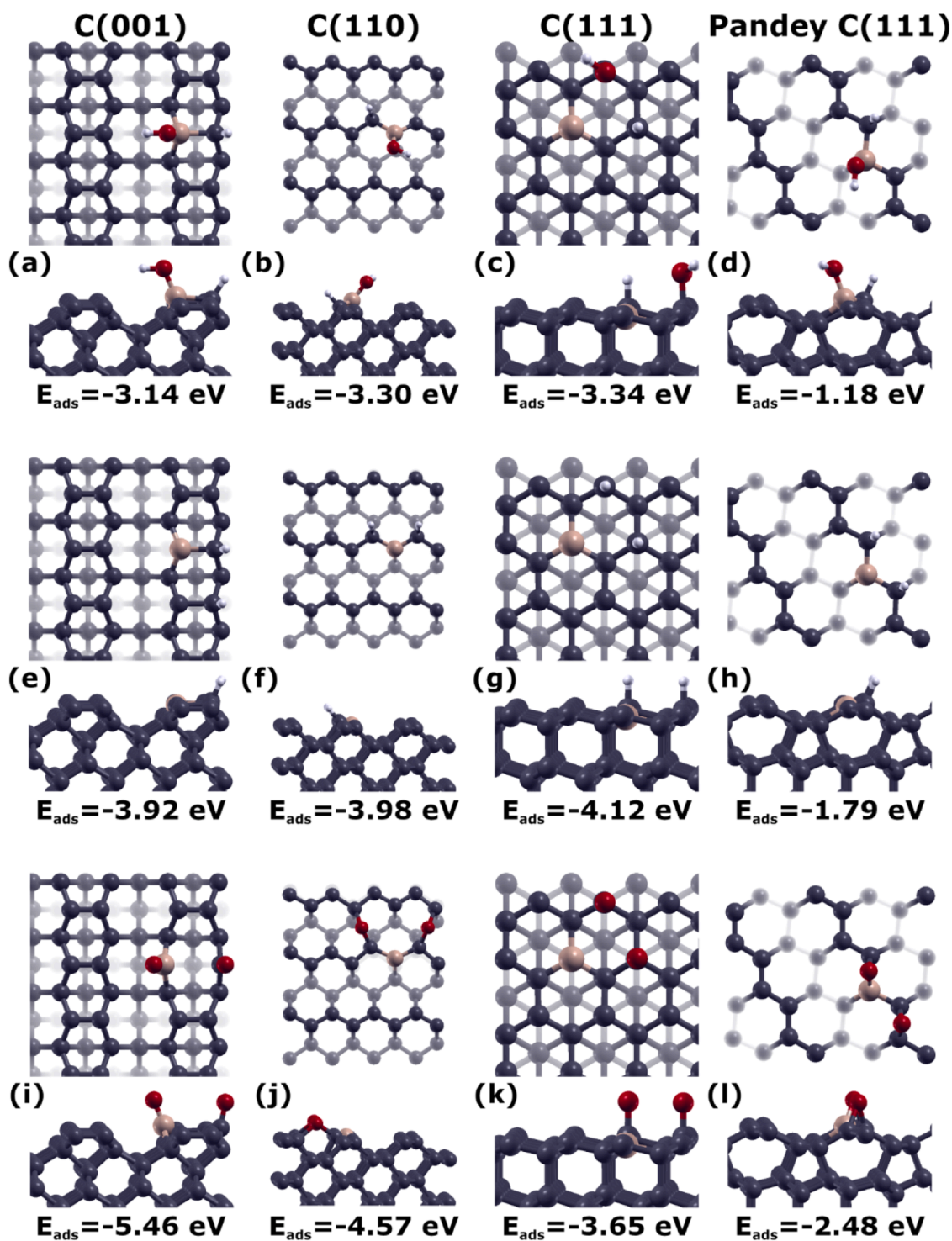
Fig. 4. Top and side view representations of the most stable configurations for the dissociative adsorption of the H_2O (a-d), H_2 (e-h) and O_2 (i-l) molecules, along with their respective adsorption energies per molecule, for the four considered surface orientations. Pink spheres correspond to the B dopants while grey spheres correspond to C atoms. H and O atoms are represented with white and red spheres, respectively. In all cases, the B dopant is positioned on the topmost atomic layer.

third atomic layer in the unreconstructed (111) surface was found to lead to a reduction of the energy gain, when H_2 is adsorbed on the vicinity of B.

Moreover, even though O_2 was found to be most preferably adsorbed in all the considered B-doped and undoped surfaces compared to H_2 and H_2O, the dissociation of H_2 on the unreconstructed (111) surface was found to lead to the highest energy gain, compared to the dissociation of the other two considered molecules (Fig. 6b). The fact that H_2 is shown

to be preferably dissociated on the unreconstructed (111) surface compared to O_2 might be interesting for applications in tribology or catalysis, in which the adsorption of oxygen species would be undesired.

3.3.3. O_2 dissociative adsorption

The dissociation of O_2 from the B-doped surfaces was found to occur in different ways, depending on the considered surface orientation, with the formation of ether-group or carbonyl-like configurations. The effect
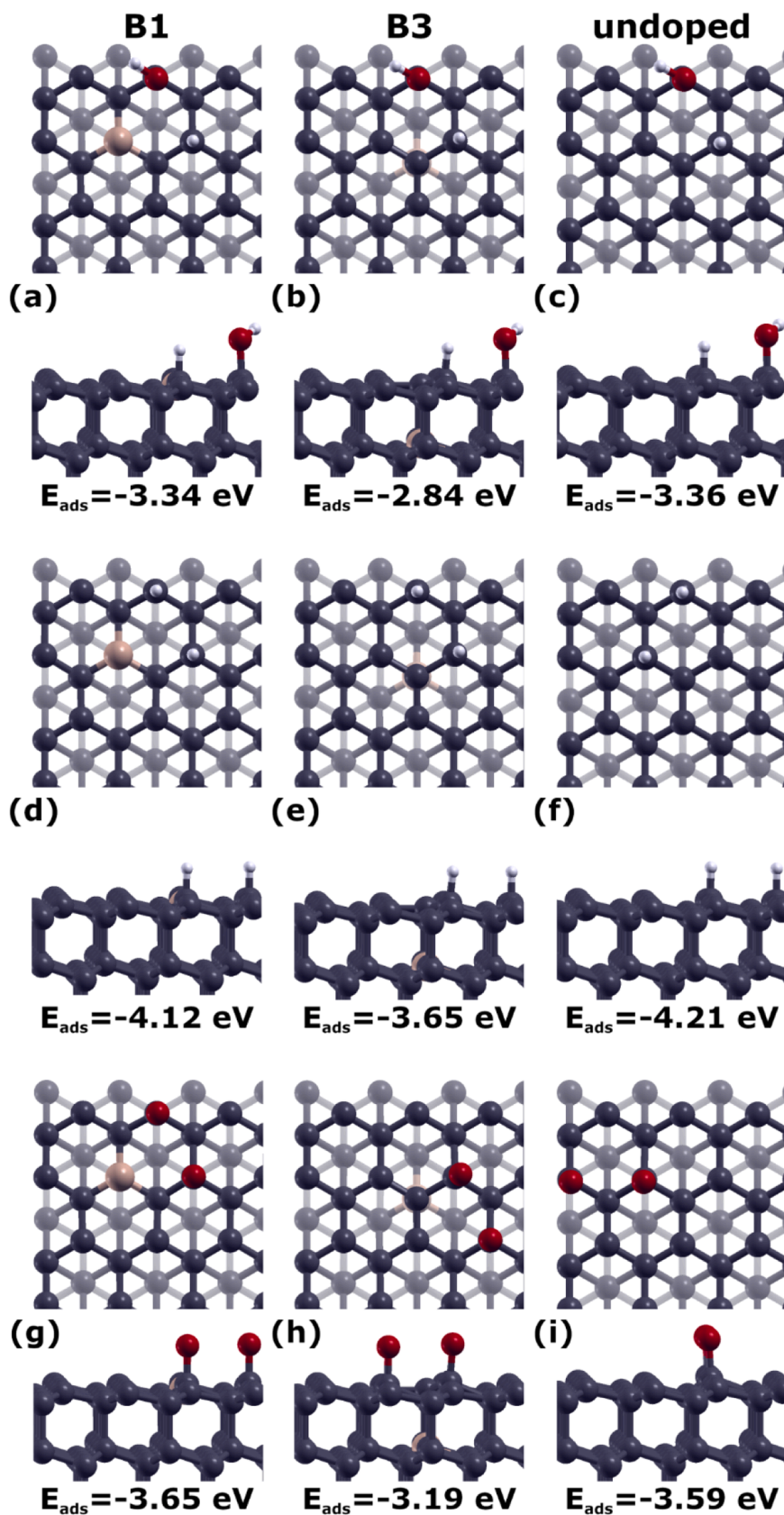
Fig. 5. Top and side view representations of the most stable configurations for the dissociative adsorption of the H_2O (a-c), H_2 (d-f) and O_2 (g-i) molecules, along with their respective adsorption energies per molecule, for the B-doped, unreconstructed C(111) surface with the B atom on the first ("B1") and third ("B3") atomic layer, and the undoped unreconstructed C(111) surface. Pink spheres correspond to the B dopants while grey spheres correspond to C atoms. H and O atoms are represented with white and red spheres, respectively.
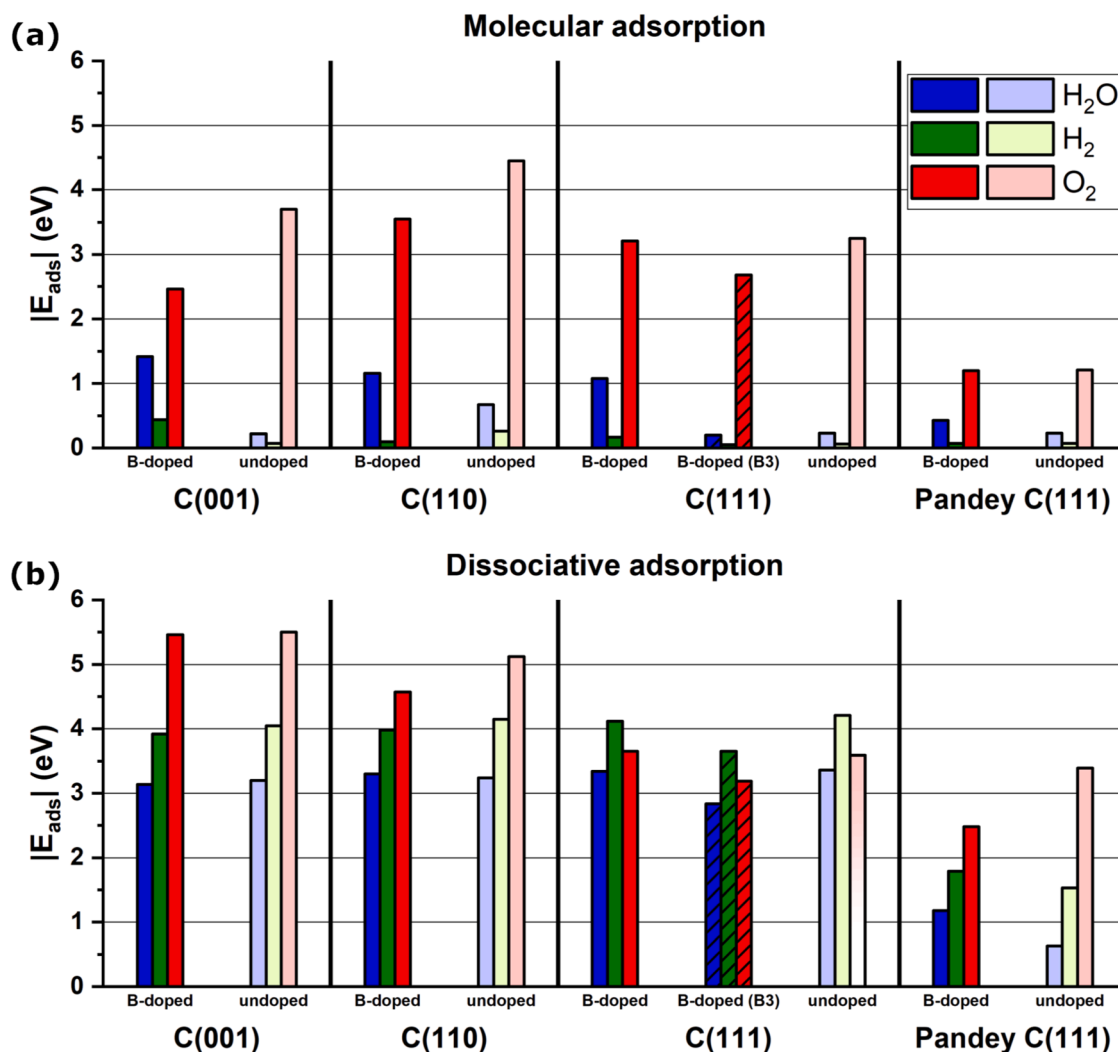
Fig. 6. Absolute values of the adsorption energies per molecule of the most stable configurations for molecular (a) and dissociative (b) adsorption of the H_2O, H_2 and O_2 molecules on the four considered surface orientations. Cases denoted as "B-doped" correspond to surfaces with the B atom on the topmost atomic layer, except for the case of C(111) surface, where also the case of the B atom in the third atomic layer ("B3") is included. Results for H_2O are represented with blue, for H_2 with green and for O_2 with red color. Lighter colors are used for the corresponding molecules on the undoped surfaces. Stripe-patterned bars in the case of the C(111) surface correspond to the "B3" case. Results for the undoped C(001), C(110) and Pandey reconstructed C(111) surfaces are taken from [45].

of B doping is evident in this type of adsorption, as in the undoped surfaces, the dissociation of O_2 was found to lead only to the formation of C—O—C ether configurations [45].

In particular, the formation of carbonyl configurations was observed in the B-doped (001) and the unreconstructed (111) surfaces. In the former case, the O fragments were found to break the B—C dimer and form double bonds with B and C. The O=B bond was observed to be longer (1.27 Å) than the O=C one (1.21 Å). The adsorption energy in this case was very close to the one of the respective undoped surface, even though in the former case, the adsorption was most stable in an ether configuration [45]. In the latter case, the adsorbed O fragments formed double-like O=C bonds with the dangling bonds of the C atoms in the second coordination shell of B, for the case of B on the surface (B1), and in the second and fourth coordination shells in the case of B in the third layer (B3), following the same pattern as in both previous cases of dissociative adsorption. The adsorption energy on the B1 case was again very close to the undoped one, but a higher value was calculated for B3. The O=C bond length in all the unreconstructed (111) surfaces was measured close to 1.35 Å.

On the other hand, the formation of ether configurations was found to be preferable for the (110) and Pandey reconstructed (111) surfaces.

In both cases, the most stable configurations were similar to the respective undoped ones from [45]. Specifically, in the (110) surface, the O fragments were attached to C atoms, in bridge sites connecting two topmost chains, while in the Pandey (111) surface, both O atoms where adsorbed in bridge positions between two consecutive B—C and C—C pairs on the same chain. The adsorption in the B-doped cases was weaker than in the undoped one for these two surfaces by approximately 2 eV.

Overall, as was also demonstrated for the undoped diamond [45], the dissociative adsorption of O_2 is the strongest among the considered molecules and adsorption types, with the adsorption energy decreasing with (001) > (110) > unreconstructed (111) > Pandey (111), both for the undoped and the B-doped configurations. Moreover, from Fig. 4(i-l), it is evident that the adsorption of the O fragments leads to the displacement of the surface atoms attached to them, mostly in the (001) and (110) configurations. Similar to the case of the dissociative adsorption of H_2O, this observation, along with the high energy gain of the O_2 adsorption (which is in general observed both for the B-doped and the undoped diamond surfaces), could also be associated to previous evidence of higher wear rates in BDD, compared to undoped diamond coatings [19]. Moreover, the formation of C—O—C pairs was experimentally found to be preferably formed in longer oxidation times

compared to C—OH, along with evidence of surface reconstruction in the former case [41], in agreement with the results of adsorption energies and most stable geometries presented here.

3.4. Reaction paths and energy barriers of H₂O dissociation on B-doped diamond surfaces

From the above, since the introduction of surface B dopants was found to affect H₂O adsorption, the H₂O dissociation reaction paths and the respective energy barriers were estimated via the NEB method. The results are shown in Figs. 7 and 8 and the overall comparison between all the B-doped and undoped considered surfaces in Fig. 9.

Regarding the C(001) surface (Fig. 7a), the calculated energy barriers are similar in the B-doped and the undoped cases, with the introduction of B leading to a small increase of the energy barrier by 0.22 eV. As demonstrated in the previous sections, B-doping was found to enhance the adsorption of the water molecule, therefore the observed increase of the energy barrier can be associated to the in-creased stability of the considered initial state of the water dissociation.

On the other hand, B-doping was found to slightly reduce the energy barrier for water dissociation on C(110), as shown in Fig. 7b. By examining the corresponding transition states, in the undoped surface, one of the two H atoms initially pointing towards the surface is detached from the water molecule and adsorbed on the surface. The latter transfer of H from the weakly physisorbed water molecule to the surface (with no intermediate chemisorption occurring, as in the previous case), can be associated with the pronounced energy barrier of the water dissociation on the undoped surface by 0.32 eV compared to the B-doped one.

Similar to the previous case, B doping was also found to reduce the energy barrier for water dissociation on the Pandey reconstructed C(111) surface, with this reduction being more pronounced in the latter case (1.07 eV), as it is shown in Fig. 7c. In both the B-doped and undoped surfaces, the water molecule is initially physisorbed. However, in the first case it dissociates through an intermediate chemisorption on the surface B atom, while in the second one, it dissociates while still in the physisorption state. The intermediate chemisorption of water on B appears to be a much favorable scenario than the direct dissociation of water while in the physisorption state (which was also the case in the adsorption on the C(110) surface), leading again to a lower energy barrier on the case of the adsorption on the B-doped surface.

The MEPs along with the respective energy barriers and initial, transition and final state configurations for the water dissociation on the B-doped (with B on the first, "B1" and third, "B3" atomic layers) and undoped unreconstructed C(111) surfaces are presented in Fig. 8a. The dissociation on the B3 surface is very similar to that on the undoped surface, as in both cases the initial state involves a physisorbed water molecule, which dissociates through the intermediate adsorption of one of its H atoms on the surface. The energy barriers in both cases are also similar (0.48 eV in the B3 and 0.41 eV in the undoped surface). However, the dissociation on the B1 surface presents a different case, as demonstrated in more detail in Fig. 8b. In this case, the water molecule is initially being chemisorbed, and consequently dissociates to the intermediate metastable dissociation state Dis-I1 through the transition state TS, with a very low energy barrier of 0.07 eV. One H atom of the water molecule is adsorbed on its nearest C atom and subsequently migrates to an adjacent C atom (intermediate metastable dissociation state Dis-I2) through the transition state TS2, with an energy barrier of 2.87 eV. Moreover, the hydroxyl fragment migrates from B to its adjacent C atom (previously occupied by H in Dis-I1) in the final, most stable dissociation state, Dis, through the transition state TS3, with an energy barrier of 1.24 eV. The two metastable intermediate dissociation states with hydroxyl adsorbed on B, Dis-I1 and Dis-I2 are less stable than the final one (with hydroxyl adsorbed on a C atom) by 0.28 eV. Therefore, it is evident that in the B1 case, water can be dissociated easily with a very low energy barrier (0.07 eV), however the most stable dissociation state can be reached by subsequent migration of the fragments on top of surface

atoms, with higher energy barriers (1.24 and 2.87 eV).

4. Conclusions

In this work, the molecular and dissociative adsorption of H₂O, H₂ and O₂ on boron doped (001), (110), and (111), both Pandey-reconstructed and unreconstructed surfaces were studied *ab initio*, in close comparison with previous results for the corresponding undoped configurations [45]. In all cases, the B dopant was found to be preferably located in a substitutional site of the topmost layer, except for the unreconstructed (111), in which it was preferably located on the third atomic layer (in agreement with previous calculations [51]). In the latter case, it was found to reduce the adsorption strength in the vicinity of its topmost atom.

The presence of B on the considered diamond surfaces was shown to lead to the formation of a dative bond with O in the molecular adsorption of H₂O, increasing the energy gain for adsorption by 0.7 eV on average, and consequently increasing the probability for H₂O molecules to be captured on the surface with respect to the undoped case. This result was in agreement with a previous *ab initio study* on the B-doped (001) surface [50], and can be associated to the observed improved friction coefficient of BDD under water lubrication [20,22]. On the other hand, the molecular adsorption of O₂ was found to be weaker on the B-doped (001) and (110) surfaces compared to the undoped ones, while on the Pandey (111), less reactive, is similar in both the cases.

Moreover, the dissociative adsorption of O₂ was also found to be slightly weaker on the (110) and Pandey (111) B-doped surfaces. In these configurations, O atoms were found to be most stable in ether-like, bridge positions, while on the (001) and unreconstructed (111) surfaces, O atoms were found at carbonyl-like, on-top positions and the adsorption strength was similar to the undoped surfaces. In the most stable adsorption configurations for O dissociation on the (001) and (110) surfaces, a pronounced displacement of the surface atoms attached to the O adsorbate was observed, which could potentially act as the source of atomistic wear mechanisms. In the dissociative adsorption of H₂O, the hydroxyl fragments were preferably attached to the B atom and the H fragments to a C atom in the first coordination shell of B in most cases, and a pronounced displacement of surface atoms attached to the adsorbed fragments was also observed in the (001), (110) and Pandey (111) surfaces. The Pandey (111) surface was again found to be the less reactive surface towards the dissociation of all the considered molecules.

Energy barriers for water dissociation were found to be lower in almost all the considered B-doped surfaces compared to the undoped ones, with the most evident difference observed for the Pandey reconstructed C(111). The C(001) surface was the only case in which the energy barrier was higher on the undoped surface, but only by 0.22 eV. In the B-doped case, the water molecule is chemisorbed in the initial state, making it very stable. A particularly low energy barrier of 0.07 eV was found for the water dissociation on the B-doped unreconstructed C(111) surface with B on the topmost layer ("B1"). This barrier corresponds to the initial dissociation of water to a metastable dissociation configuration with hydroxyl attached on B. The most stable dissociation configuration which involves both H and OH fragments adsorbed on surface C atoms, can be reached from the metastable one through consequent surface migrations, which are associated with high energy barriers.

These results aim to provide a quantitative and qualitive understanding of the impact of boron doping on the atomistic mechanisms of adsorption of H₂O, H₂ and O₂ on the most common diamond surfaces. The direct comparison with the adsorption results for the clean undoped diamond in [45] demonstrated the role of surface B in these interactions. In particular, the enhanced adsorption of water molecules due to exposed surface B can have implications in tribochemical reactions, explaining the reduced COF that has been experimentally observed in BDD coatings, particularly in wet ambient conditions [18,19,22]. The ultralow COF and self-lubricating properties of undoped diamond, due
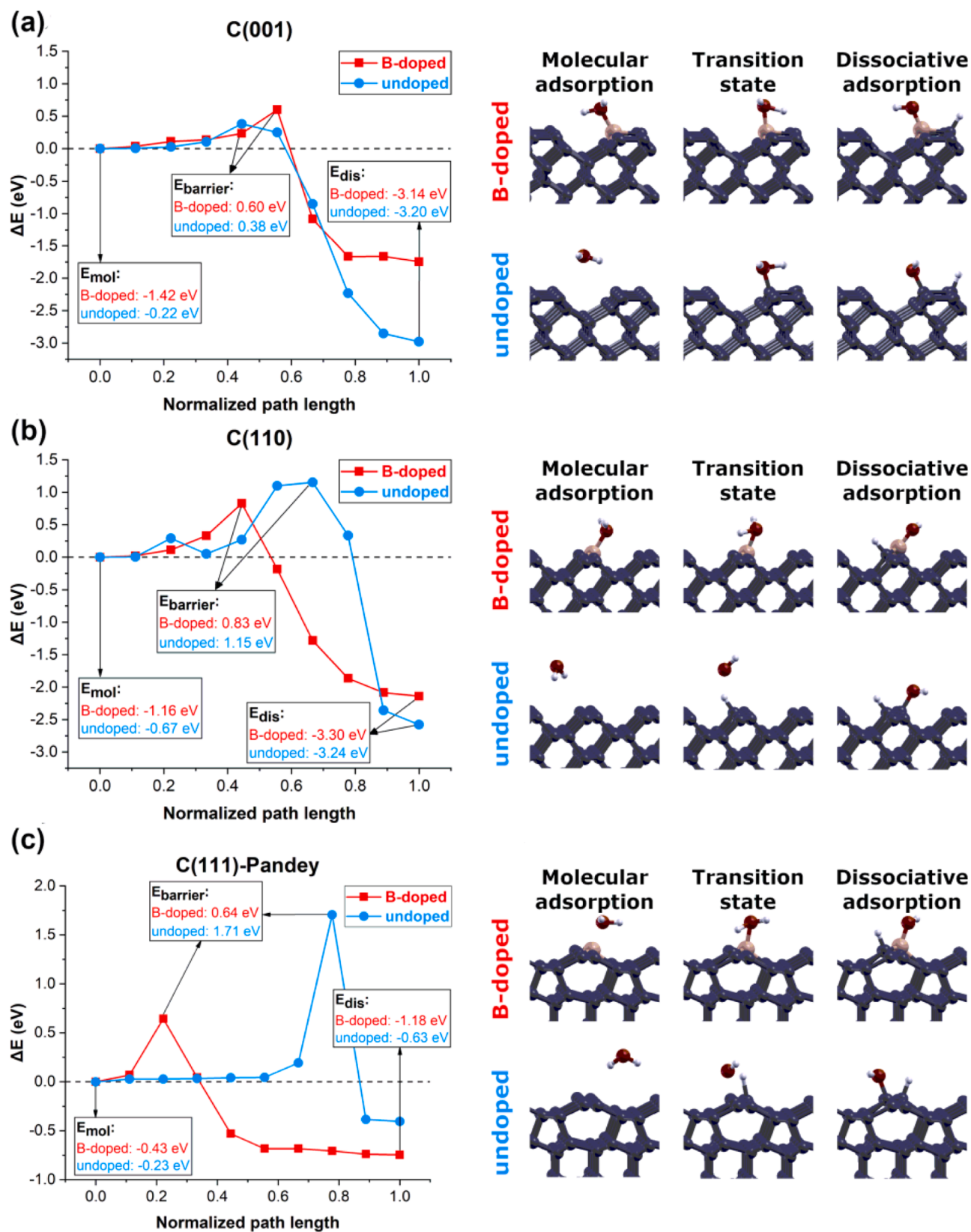
Fig. 7. Minimum energy paths and the respective energy barriers, along with the corresponding molecular and dissociative adsorption energies from [45], for the dissociation of water on the B-doped (red, squares) and the respective undoped (blue, circles) C(001) (a), C(110) (b) and Pandey reconstructed C(111) surfaces (left). Structural configurations of the initial (molecular adsorption), transition and final (dissociative adsorption) states of water dissociation on the B-doped (top) and undoped (bottom) C(001) (a), C(110) (b) and Pandey reconstructed C(111) surfaces (right).
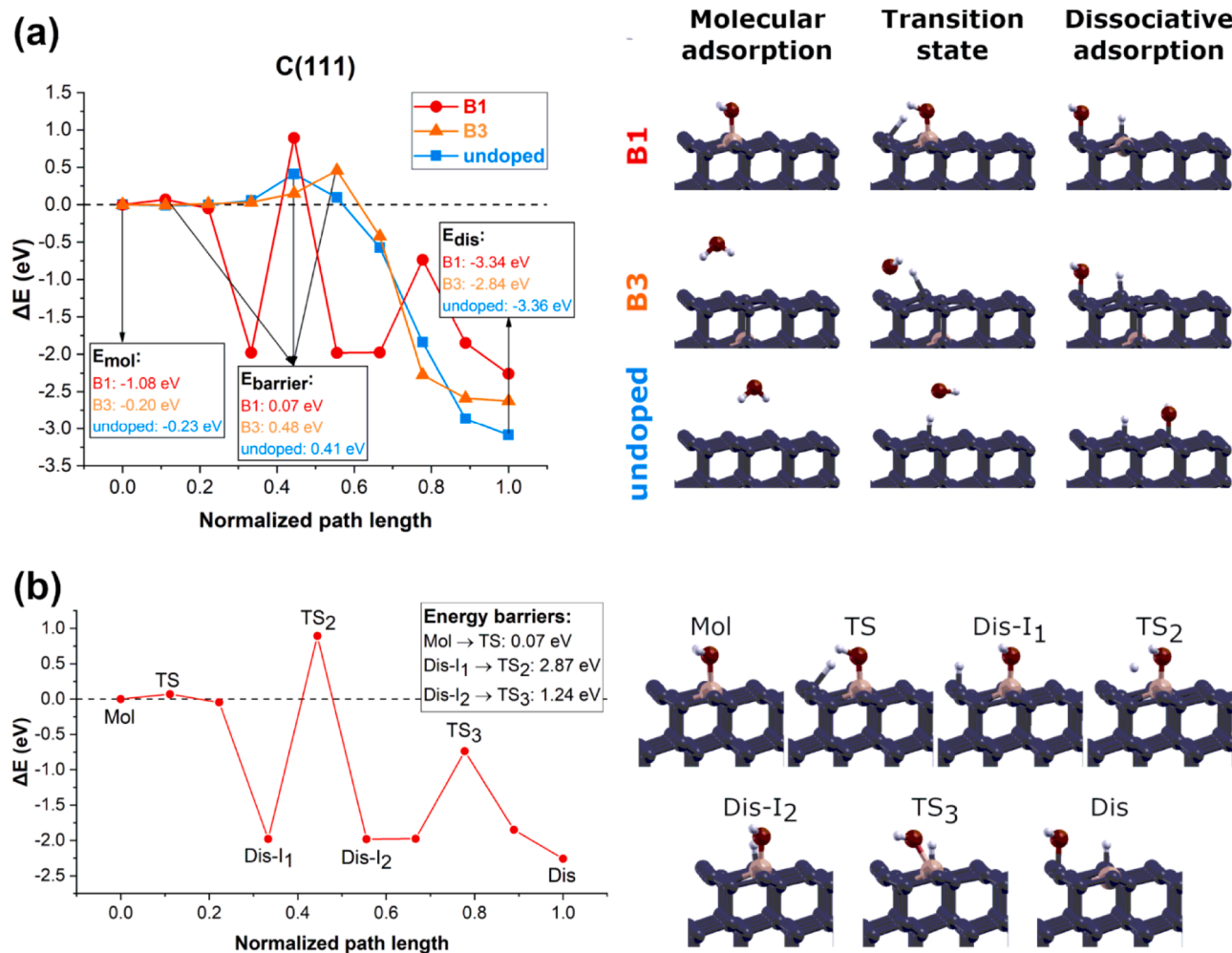
Fig. 8. (a) Minimum energy paths and the respective energy barriers, along with the corresponding molecular and dissociative adsorption energies from [45], for the dissociation of water on the B-doped at B1 (red, circles) and B3 (orange, triangles) sites and the respective undoped (blue, squares) unreconstructed C(111) surfaces (left). Structural configurations of the initial (molecular adsorption), transition and final (dissociative adsorption) states of water dissociation on the B-doped (top) and undoped (bottom) unreconstructed C(111) surfaces (right). (b) Minimum energy path for the dissociation of water on the B1-C(111) surface and structural configurations for the initial molecular adsorption ("Mol"), transition ("TS"), first intermediate dissociative adsorption ("Dis-I1"), second transition ("TS2"), second intermediate dissociative adsorption ("Dis-I2"), third transition ("TS3") and final dissociative adsorption ("Dis") states. The respective energy barriers for each transition are included in the top inset.
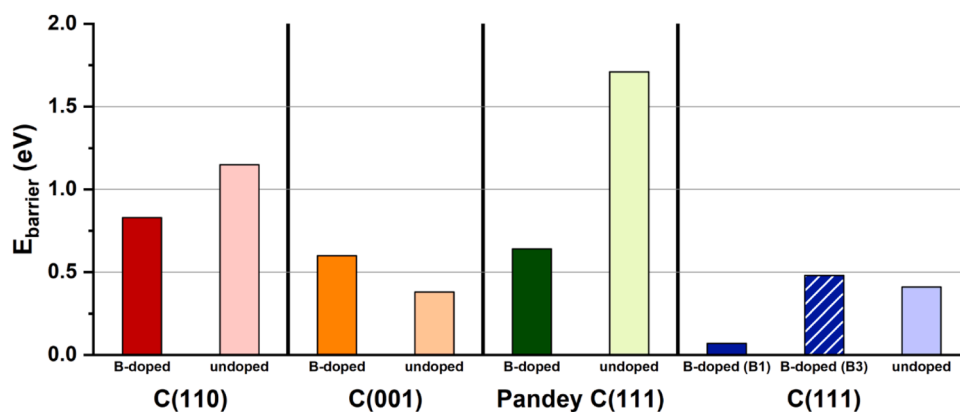

Fig. 9. Comparative representation of the calculated energy barriers for water splitting in the B-doped and undoped C(001) (red), C(110) (orange), Pandey reconstructed (green) and unreconstructed C(111) (blue) surfaces. Dark colours denote the B-doped while light colours denote the undoped systems.

to the tribochemically activated dissociation of ambient air molecules and the subsequent passivation of surface dangling bonds, have been widely reported both experimentally and theoretically [6–14], thus the

enhancement of water absorption from surface B demonstrated in this work can be associated to the reduced COF in BDD coatings via the augmentation of similar phenomena. Moreover, the interaction of BDD

with water is important in electrochemical reactions, as for instance physisorbed active hydroxyl radicals, electro-generated from water molecules, but also chemisorbed oxygen species, are used to attack organic pollutants in wastewater treatment applications [32]. Finally, the assessment of the adsorption properties of the clean surface (which can be produced during growth by abstraction reactions) can also be useful for designing strategies for controlling and modifying surface termination. Thus, the present theoretical analysis of the fundamental mechanisms of adsorption will hopefully motivate further research towards improving the controlled use of B-doping in tribological, electrochemical and other technological applications of diamond.

CRediT authorship contribution statement

Stefanos Giaremis: Writing – review & editing, Writing – original draft, Visualization, Validation, Investigation, Formal analysis. **Maria Clelia Righi:** Writing – review & editing, Writing – original draft, Validation, Supervision, Resources, Project administration, Funding acquisition, Conceptualization.

Declaration of competing interest

The authors declare that they have no known competing financial interests or personal relationships that could have appeared to influence the work reported in this paper

Data availability

Data will be made available on request.

Acknowledgements

References

[1] E. Salgueiredo, F.A. Almeida, M. Amaral, M.A. Neto, F.J. Oliveira, R.F. Silva, A multilayer approach for enhancing the erosive wear resistance of CVD diamond coatings, Wear 297 (2013) 1064–1073.

[2] R. Dumpala, N. Kumar, C.R. Kumaran, S. Dash, B. Ramamoorthy, M.S. Ramachandra Rao, Adhesion characteristics of nano- and micro-crystalline diamond coatings: Raman stress mapping of the scratch tracks, Diam. Relat. Mater. 44 (2014) 71–77.

[3] S. Handschuh-Wang, T. Wang, L. Zhu, Y. Xu, L. Huang, T. Gan, Y. Tang, X. Zhou, Corrosion-resistant functional diamond coatings for reliable interfacing of liquid metals with solid metals, ACS Appl. Mater. Interfaces 12 (2020) 40891–40900.

[4] T. Wang, L. Huang, Y. Liu, X. Li, C. Liu, S. Handschuh-Wang, Y. Xu, Y. Zhao, Y. Tang, Robust biomimetic hierarchical diamond architecture with a self-cleaning, antibacterial, and antibiofouling surface, ACS Appl. Mater. Interfaces 12 (2020) 24432–24441.

[5] A. Tyagi, R.S. Walia, Q. Murtaza, Tribological behavior of temperature dependent environment friendly.

[6] A.R. Konicek, D.S. Grierson, P.U.P.A. Gilbert, W.G. Sawyer, A.V. Sumant, R.W. Carpick, Origin of ultralow friction and wear in ultrananocrystalline diamond, Phys. Rev. Lett. 100 (2008) 235502.

[7] G. Zilibotti, M.C. Righi, Ab initio calculation of the adhesion and ideal shear strength of planar diamond interfaces with different atomic structure and hydrogen coverage, Langmuir 27 (11) (2011) 6862–6867.

[8] M.-I.D.B. Bouchet, G. Zilibotti, C. Matta, M.C. Righi, L. Vandenbulcke, B. Vacher, J.-M. Martin, Friction of diamond in the presence of water vapor and hydrogen gas. Coupling gas-phase lubrication and first-principles studies, J. Phys. Chem. C 116 (2012) 6966–6972.

[9] G. Zilibotti, S. Corni, M.C. Righi, Load-induced confinement activates diamond lubrication by water, Phys. Rev. Lett. 111 (2013) 146101.

[10] A.R. Konicek, D.S. Grierson, A.V. Sumant, T.A. Friedmann, J.P. Sullivan, P.U.P.A. Gilbert, W.G. Sawyer, R.W. Carpick, Influence of surface passivation on the friction and wear behavior of ultrananocrystalline diamond and tetrahedral amorphous carbon thin films, Phys. Rev. B 85 (2012) 155448.

[11] T. Kuwahara, G. Moras, M. Moseler, Role of oxygen functional groups in the friction of water-lubricated low-index diamond surfaces, Phys. Rev. Mater. 2 (2018) 073606.

[12] S.R. Polaki, N. Kumar, K. Madapu, K. Ganesan, N.G. Krishna, S.K. Srivastava, S. Abhaya, S.Dash M.Kamruddin, A.K. Tyagi, Interpretation of friction and wear in DLC film: role of surface chemistry and test environment, J. Phys. D 49 (2016) 445302.

[13] X. Lei, B. Shen, S. Chen, L. Wang, F. Sun, Tribological behavior between micro- and nano-crystalline diamond films under dry sliding and water lubrication, Tribol. Int. 69 (2014) 118–127.

[14] N. Kumar, R. Ramadoss, A.T. Kozakov, K.J. Sankaran, S. Dash, A.K. Tyagi, N.H. Tai, I.-N. Lin, Humidity-dependent friction mechanism in an ultrananocrystalline diamond film, J. Phys. D 46 (2013) 275501.

[15] L. Huang, T. Wang, X. Li, X. Wang, W. Zhang, Y. Yang, Y. Tang, UV-to-IR highly transparent ultrathin diamond nanofilms with intriguing performances: anti-fogging, self-cleaning and self-lubricatin, Appl. Surf. Sci. 527 (2020) 146733.

[16] K. Ramasubramanian, N. Arunachalam, M.S. Ramachandra Rao, Investigation on tribological behaviour of boron doped diamond coated cemented tungsten carbide for cutting tool applications, Surf. Coat. Technol. 332 (2017) 332–340.

[17] D. Xiang, Z. Su, Y. Li, Z. Zhang, The effect of laser texture on adhesion and tribological properties of boron-doped diamond film on WC-Co cemented carbide, Diam. Relat. Mat. 130 (2022) 109469.

[18] S. Liza, J. Hieda, H. Akasaka, N. Ohtake, Y. Tsutsumi, Akiko Nagai, Takao Hanawa, Deposition of boron doped DLC films on TiNb and characterization of their mechanical properties and blood compatibility, Sci. Technol. Adv. Mater. 18 (1) (2017) 76–87.

[19] Q. Liang, A. Stanishevsky, Y.K. Vohra, Tribological properties of undoped and boron-doped nanocrystalline diamond films, Thin Solid Films 517 (2008) 800–804.

[20] D. Xiang, Z. Zhang, Y. Chen, Y. Hu, X. Lei, Study of tribological properties of textured boron-doped diamond film under water lubrication, Surf. Interfaces 23 (2021) 100983.

[21] J.G. Buijnsters, M. Tsigkourakos, T. Hantschel, F.O.V. Gomes, T. Nuytten, P. Favia, H. Bender, K. Arstila, J.-P. Celis, W. Vandervorst, Effect of boron doping on the wear behavior of the growth and nucleation surfaces of micro- and nanocrystalline diamond films, ACS Appl. Mater. Interfaces 8 (39) (2016) 26381–26391.

[22] M. Lu, H. Wang, X. Song, F. Sun, Effect of doping level on residual stress, coating-substrate adhesion and wear resistance of boron-doped diamond coated tools, J. Manuf. Process 88 (2023) 145–156.

[23] C.J.H. Wort, R.S. Balmer, Diamond as an electronic material, Mater. Today 11 (1-2) (2008) 22–28.

[24] A. Fujishima, Y. Einaga, T.N. Rao, D.A. Tryk, Diamond Electrochemistry, Elsevier, 2005.

[25] G. Braunstein, R. Kalish, Effective p-type doping of diamond by boron ion implantation.

[26] A.W. Williams, E.C. Lightowl, A.T. Collins, Impurity conduction in synthetic semiconducting diamond, J. Phys. C 3 (1970) 1727.

[27] M. Bernard, A. Deneuville, P. Muret, Non-destructive determination of the boron concentration of heavily doped metallic diamond thin films from Raman spectroscopy, Diam. Relat. Mat. 13 (2004) 282.

[28] F. Pruvost, E. Bustarret, A. Deneuville, Characteristics of homoepitaxial heavily boron-doped diamond films from their Raman spectra Diam, Relat. Mat. 9 (2000) 295.

[29] C. Levy-Clement, Semiconducting and metallic boron-doped diamond electrodes, in: A. Fujishima, Y. Einaga, T.N. Rao, D.A. Tryk (Eds.), Diamond Electrochemistry, Elsevier, Amsterdam, 2005, p. 80.

[30] N. Yang, J.S. Foord, X. Jiang, Diamond electrochemistry at the nanoscale: a review, Carbon 99 (2016) 90–110.

[31] R. Bogdanowicz, J. Ryl, Structural and electrochemical heterogeneities of boron-doped diamond surfaces, Curr. Opin. Electrochem. 31 (2022) 100876.

[32] P.V. Nidheesh, G. Divyapriya, N. Oturan, C. Trellu, M.A. Oturan, Environmental applications of boron-doped diamond electrodes: 1. Applications in water and wastewater treatment, ChemElectroChem 6 (8) (2019) 2124–2142.

[33] J.V. Macpherson, A practical guide to using boron doped diamond in electrochemical research, Phys. Chem. Chem. Phys. 17 (2015) 2935–2949.

[34] T.A. Ivandini, Y. Einaga, Polycrystalline boron-doped diamond electrodes for electrocatalytic and electrosynthetic applications, Chem. Commun. 53 (2017) 1338–1347.

[35] Y. He, H. Lin, Z. Guob, W. Zhang, H. Lid, W. Huang, Recent developments and advances in boron-doped diamond electrodes for electrochemical oxidation of organic pollutants, Sep. Purif. Technol. 212 (2019) 802–821.

[36] T. Yano, D.A. Tryk, K. Hashimoto, A. Fujishima, Electrochemical Behavior of Highly Conductive Boron-Doped Diamond Electrodes for Oxygen Reduction in Alkaline Solution, J. Electrochem. Soc. 145 (1998) 1870.

[37] H.B. Martin, A. Argoitia, U. Landau, A.B. Anderson, J.C. Angus, Hydrogen and oxygen evolution on boron-doped diamond electrodes, J. Electrochem. Soc. 143 (1996) L133.

[38] R. Hoffmann, A. Kriele, H. Obloh, J. Hees, M. Wolfer, W. Smirnov, N. Yang, C.E. Nebel, Electrochemical hydrogen termination of boron-doped diamond, Appl. Phys. Lett. 97 (2010) 052103.

[39] F. Liu, J. Wang, B. Liu, X. Li, D. Chen, Effect of electronic structures on electrochemical behaviors of surface-terminated boron-doped diamond film electrodes, Diam. Relat. Mater. 16 (2007) 454–460.

[40] M.C. James, F. Fogarty, R. Zulkharnay, N.A. Fox, P.W. May, A review of surface functionalisation of diamond for thermionic emission applications, Carbon 171 (2021) 532–550.

[41] M. Wang, N. Simon, C. Decorse-Pascanut, M. Bouttemy, A. Etcheberry, M. Li, R. Boukherroub, S. Szunerits, Comparison of the chemical composition of boron-doped diamond surfaces upon different oxidation processes, Electrochim. Acta 54 (2009) 5818–5824.

[42] G. Levita, S. Kajita, M.C. Righi, Water adsorption on diamond (111) surfaces: an ab initio study, Carbon 125 (2018) 533–540.

[43] G. Zilibotti, M.C. Righi, M. Ferrario, *Ab initio* study on the surface chemistry and nanotribological properties of passivated diamond surfaces, Phys. Rev. B 79 (2009) 075420.

[44] D. Petrini, K. Larsson, Theoretical study of the thermodynamic and kinetic aspects of terminated (111) diamond surfaces, J. Phys. Chem. C 112 (8) (2008) 3018–3026.

[45] N.V. Tran, M.C. Righi, Ab initio insights into the interaction mechanisms between H_2, H_2O, and O_2 molecules with diamond surfaces, Carbon 31 (199) (2022) 497–507.

[46] J.I. Enriquez, F. Muttaqien, M. Michiuchi, K. Inagaki, M. Geshi, I. Hamada, Y. Morikawa, Oxidative etching mechanism of the diamond (100) surface, Carbon 174 (2021) 36–51.

[47] M. Cutini, G. Forghieri, M. Ferrario, M.C. Righi, Adhesion, friction and tribochemical reactions at the diamond–silica interface, Carbon 203 (2023) 601–610.

[48] S. Kajita, M.C. Righi, A fundamental mechanism for carbon-film lubricity identified by means of *ab initio* molecular dynamics, Carbon 103 (2016) 193–199.

[49] S. Zhao, K. Larsson, Theoretical study of the energetic stability and geometry of terminated and B-doped diamond (111) surfaces, J. Phys. Chem. C 118 (4) (2014) 1944–1957.

[50] C.A. Latorre, J.P. Ewen, D. Dini, M.C. Righi, Ab initio insights into the interaction mechanisms between boron, nitrogen and oxygen doped diamond surfaces and water molecules, Carbon 171 (2021) 575–584.

[51] R. Jaimes, J. Vazquez-Arenas, I. González, M. Galván, Delimiting the boron influence on the adsorptive properties of water and •OH radicals on H-terminated boron doped diamond catalysts: a density functional theory analysis, Surf. Sci. 653 (2016) 27–33.

[52] T.A. Ivandini, T. Watanabe, T. Matsui, Y. Ootani, S. Iizuka, R. Toyoshima, H. Kodama, H. Kondoh, Y. Tateyama, Y. Einaga, Influence of surface orientation on electrochemical properties of boron-doped diamond, J. Phys. Chem. C 123 (2019) 5336–54344.

[53] B.D. Thoms, J.N. Russell Jr, P.E. Pehrsson, J.E. Butler, Adsorption and abstraction of hydrogen on polycrystalline diamond, J. Chem. Phys. 100 (1994) 8425–8431.

[54] B.N. Jariwala, C.V. Ciobanu, S. Agarwal, Facile abstraction of hydrogen atoms from graphene, diamond, and amorphous carbon surfaces: a first-principles study, Phys. Rev. B 82 (2010) 085418.

[55] R. Giro, P.W. Bryant, M. Engel, R.F. Neumann, M.B. Steiner, Adsorption energy as a metric for wettability at the nanoscale, Sci. Rep. 7 (2017) 46317.

[56] P. Giannozzi, S. Baroni, N. Bonini, M. Calandra, R. Car, C. Cavazzoni, D. Ceresoli, G.L. Chiarotti, M. Cococcioni, I. Dabo, A. Dal Corso, S. Fabris, G. Fratesi, S. de Gironcoli, R. Gebauer, U. Gerstmann, C. Gougoussis, A. Kokalj, M. Lazzeri, L. Martin-Samos, N. Marzari, F. Mauri, R. Mazzarello, S. Paolini, A. Pasquarello,

L. Paulatto, C. Sbraccia, S. Scandolo, G. Sclauzero, A.P. Seitsonen, A. Smogunov, P. Umari, R.M. Wentzcovitch, QUANTUM ESPRESSO: a modular and open-source software project for quantum simulations of materials, J. Phys. 21 (2009) 395502.

[57] D. Vanderbilt, Soft self-consistent pseudopotentials in a generalized eigenvalue formalism, Phys. Rev. B 41 (11) (1990) 7892(R).

[58] J.P. Perdew, K. Burke, M. Ernzerhof, Generalized gradient approximation made simple, Phys. Rev. Lett. 77 (18) (1996) 3865–3868.

[59] S. Grimme, Semiempirical GGA-type density functional constructed with a long-range dispersion correction, J. Comput. Chem. 27 (15) (2006) 1787–1799.

[60] V. Barone, M. Casarin, D. Forrer, M. Pavone, M. Sambi, A. Vittadini, Role and effective treatment of dispersive forces in materials: polyethylene and graphite crystals as test cases, J. Comput. Chem. 30 (2009) 934–939.

[61] H.J. Monkhorst, J.D. Pack, Special points for Brillouin-zone integrations, Phys. Rev. B 13 (1976) 5188–5192.

[62] A. Kokalj, Computer graphics and graphical user interfaces as tools in simulations of matter at the atomic scale, Comput. Mater. Sci. 28 (2) (2003) 155–168.

[63] L.T. Anh, F. Celine, I. Catalan, Y. Kim, Y. Einaga, Y. Tateyama, Boron position-dependent surface reconstruction and electronic states of boron-doped diamond (111) surfaces: an ab initio study, Phys. Chem. Chem. Phys. 23 (2021) 15628–15634.

[64] R. Samlenski, C. Haug, R. Brenn, C. Wild, R. Locher, P. Koidl, Characterisation and lattice location of nitrogen and boron in homoepitaxial CVD diamond, Diam. Relat. Mater. 5 (1996) 947–951.

[65] T. Watanabe, S. Yoshioka, T. Yamamoto, H. Sepehri-Amin, T. Ohkubo, S. Matsumura, Y. Einaga, The local structure in heavily boron-doped diamond and the effect this has on its electrochemical properties, Carbon 137 (2018) 333–342.

[66] J. Xu, Y. Yokota, R.A. Wong, Y. Kim, Y. Einaga, Unusual electrochemical properties of low-doped boron-doped diamond electrodes containing sp^2 carbon, J. Am. Chem. Soc. 142 (2020) 2310–2316.

[67] G. Mills, H. Jónsson, Quantum and thermal effects in H_2 dissociative adsorption: evaluation of free energy barriers in multidimensional quantum systems, Phys. Rev. Lett. 72 (1994) 1124–1127.

[68] G. Henkelman, B.P. Uberuaga, H. Jónsson, A climbing image nudged elastic band method for finding saddle points and minimum energy paths, J. Chem. Phys. 113 (2000) 9901–9904.

[69] J. Emsley, The Elements, 3rd ed., Clarendon Press, Oxford, 1998.

[70] C. Lu, Z.L. Wang, L.F. Xu, H.X. Yang, J.J. Li, C.Z. Gu, The metallicity of B-doped diamond surface by first-principles study, Diam. Relat. Mater. 19 (2010) 824–828.

[71] M. Lu, D. Liu, C. Zhang, F. Sun, DFT calculations and experiments of oxidation resistance research on B, N, and Si multi-doped diamond films, Appl. Surf. Sci. 612 (2023) 155865.

[72] M.H.P. Santana, L.A. De Faria, J.F.C. Boodts, Electrochemical characterisation and oxygen evolution at a heavily boron doped diamond electrode, Electrochim. Acta 50 (2005) 2017–2027.

[73] P.A. Michaud, M. Panizza, L. Ouattara, T. Diaco, G. Foti, Ch. Cominellis, Electrochemical oxidation of water on synthetic boron-doped diamond thin film anodes, J. Appl. Electrochem. 33 (2003) 151–154.

[74] J. van der Weide, R.J. Nemanich, Argon and hydrogen plasma interactions on diamond (111) surfaces: electronic states and structure, Appl. Phys. Lett. 62 (1993) 1878.